Double-Pulse Laser Micro Sintering: Experimental Study and Mechanism Analysis Aided by In-situ Time-resolved Temperature Measurements

Weidong Liu, Hanyu Song, Benxin Wu*, and Haoxuan You

School of Mechanical Engineering, Purdue University, West Lafayette IN, USA

Abstract: Laser micro sintering (LMS) is a process of manufacturing microscale parts and/or features by laser sintering. Small powder particles (e.g., on the order of ~1 micron) are often used for good spatial resolutions. Besides, pulsed lasers are often employed due to related potential advantages. For good mechanical properties, pulsed laser-based LMS typically desires high densification of sintered material, which is, however, often more difficult to achieve than conventional macro selective laser sintering or melting. A new double-pulse laser micro sintering (DP-LMS) process was recently proposed by the corresponding author, which is a novel approach to potentially achieve good densification of sintered material in pulsed laser-based LMS. It employs laser pulse groups, each of which contains "sintering laser pulse(s)" followed by "pressing laser pulse(s)" at a certain delay time, which are used to sinter (melt and coalesce) the powder particles and generate a high transient pressure onto the material, respectively. This paper reports a study of the DP-LMS process for single-track sintering. The related fundamental mechanisms are analyzed with the help of in-situ time-resolved measurements of powder bed surface temperatures during DP-LMS. Under the conditions studied, it has been found that DP-LMS can produce better sintering results than those by LMS only using the sintering or pressing laser pulses. For a good sintering result in DP-LMS, the "pressing laser pulse" needs to have a sufficiently high intensity and follow the last preceding "sintering pulse" close enough such that the irradiated surface region is still in a molten state (or partially so to a sufficient extent). The fundamental mechanism for good sintering results in DP-LMS is expected to be that the 'pressing laser pulse" can induce (likely via laser ablation and plasma generation) high pressures on the powder bed surface, which can promote melt flow, reduce balling and/or enhance material densification and/or continuity. In addition, a thermal accumulation effect between adjacent "sintering laser pulses" during DP-LMS has been revealed by the in-situ temperature measurements.

Keywords: Laser micro sintering, laser micro melting, double pulse, additive manufacturing

1. Introduction

Selective laser sintering (SLS) and selective laser melting (SLM) are important additive manufacturing technologies with several advantages such as good flexibility in the geometry and

* Corresponding author: Benxin Wu, Associate Professor, School of Mechanical Engineering, Purdue University, 585 Purdue Mall, West Lafayette, IN 47907, USA, email: wu65@purdue.edu

composition of produced parts and short lead time [1-3]. Laser sintering or melting also sees applications in the fabrication of flexible electronics [4] and composites [5]. Laser micro sintering (LMS) is a process of manufacturing microscale parts and/or features by laser sintering [6-11]. It may benefit industrial areas that desire rapid and flexible production of micro parts and/or features (for simplicity in this paper, the phrase "laser sintering" will be used to refer to all processes of laser irradiation-induced powder particle coalition, regardless of whether or not powder full melting occurs).

In LMS, to get a good spatial resolution very fine powders with particle diameters on the order of ~1 μm are often used [10]. Besides, LMS by short laser pulses (e.g., with a pulse duration on the order of 100 ns) have potential advantages such as good resolution and possible prevention or reduction of surface oxidation even in air [6, 10]. For good mechanical properties, pulsed laser-based LMS typically desire a high densification of the sintered material, which is, however, often more difficult to achieve than conventional macro SLS or SLM. In particular, the powder sizes in LMS (often on the order of ~1 μm) are typically much smaller than those for the conventional macro SLS or SLM [10]. The large surface-to-volume ratios of the particles make the ratios of the inter-particle surface force over the gravity force large [6]. Hence, the particles are prone to forming agglomerated clusters and typically have a low pre-sintering apparent density in the powder bed, which may lead to the formation of spheres (i.e., balling) and/or poor densification in the sintered medium [6, 10].

The corresponding author of this paper proposed a new "double-pulse laser micro sintering" (DP-LMS) process [12, 13]. It is a novel approach to potentially achieve good densification of sintered material in pulsed laser-based LMS. The word "double" means two **types** of laser pulses are used. In DP-LMS, laser sintering is conducted using "laser pulse groups", and

each group consists of N_1 "sintering laser pulses" followed by N_2 "pressing laser pulses" at a certain delay time (where N_1 and $N_2 \geq 1$). The parameters of the "sintering laser pulses" are selected for the purpose of "sintering", i.e., to induce sufficient melting and coalition of powder particles ("target') without too much material removal. Hence, the "sintering pulses" should often have a relatively long pulse duration and a low intensity. The parameters of the "pressing laser pulse(s)" are selected for the purpose of pressing the target material, typically by the high pressure exerted on the target surface due to plasma induced by laser ablation. Hence, the "pressing pulse(s)" should often have a relatively high intensity (to induce a high pressure) and a short duration (to avoid too much energy input and material removal). DP-LMS has good process flexibility and adjustability: the parameters for the "sintering pulses" and "pressing pulses" can be selected for the purpose of sintering and pressing, respectively. The delay time of the "pressing pulse(s)" after the "sintering pulses" in each group can also be adjusted to potentially improve sintering results. The DP-LMS process utilizes special pulse formats *during* sintering to potentially enhance manufacturing performance. DP-LMS itself does *not* involve additional pre- or post-sintering treatment step(s) that may obviously increase the total production time. On the other hand, DP-LMS does not necessarily preclude these treatments (e.g., pre-sintering high-pressure compression of the powder that may benefit sintering [10]) and can be combined with them (when necessary and suitable) to potentially further improve the overall additive manufacturing performance.

A preliminary experimental study on the DP-LMS process by the authors was reported in [13]. Under the conditions investigated, optical microscopic images show that DP-LMS using laser pulse groups with 10 "sintering pulses" followed by 1 "pressing pulse" in each group can produce sintered material that appear to be much more continuous and densified with much less severe

balling than that by LMS only using the "sintering pulses". This has demonstrated a great potential of the novel DP-LMS process in the field.

However, the authors' previous experimental study on the novel DP-LMS process in [13] is very preliminary. Laser sintering was conducted at 3×3 location points on the powder surface. One laser pulse group was fired at each location point by a *stationary* laser beam. Then the beam moved to the next location point to fire the next laser pulse group. No comprehensive study was performed in [13] on the effects of major process parameters in DP-LMS.

This paper reports the authors' experimental study of the novel DP-LMS process for single-track sintering by a moving laser beam, with different values of the major parameters, such as the "pressing laser pulse" energy, delay time and the temporal distance between adjacent laser pulse groups. The sintered material lines were observed by an optical and/or scanning electron microscope for material surface morphology, continuity, densification and possible defects such as pores and balling. LMS only using the sintering or pressing laser pulses was also conducted. Sintering results under different conditions were compared.

To help analyze some related fundamental mechanisms during DP-LMS, in-situ time-resolved measurements of powder-bed surface temperature histories were performed. Such measurements are challenging due to the high spatial and temporal resolution requirements. To overcome the challenges, a two-color pyrometry system set up by the authors was used. The temperature measurement system has the advantages of non-contact and reasonably high spatial and temporal resolutions. In addition, by measuring thermal radiation in two wavelength ranges, the pyrometry system does not require the target surface emissivity values. Some related fundamental mechanisms for DP-LMS will be analyzed with the help of the in-situ temperature

measurement results. It is beyond the scope of this paper to study the achievable spatial resolution for DP-LMS.

2. Experiments

2.1 Sintering Experiments

Figure 1a and 1b show the experimental setup in this study and the laser pulse format used (it should be noted that the schematic diagrams in this paper do not necessarily include all components and do not necessarily show the exact actual details). In Fig.1a, the "sintering pulses" come from Laser 1 (SPI, G3.0, SP-20P-0008-002) with a total pulse duration of ~200 ns per pulse and a wavelength of ~1064 nm, while the "pressing pulses" come from Laser 2 (Bright Solutions, Onda) with a full-width-at-half-maximum (FWHM) duration of ~4 ns and a wavelength of ~1064 nm. The two laser beams' paths are combined through the beam splitter and then they enter the laser scan head (Scanlab, Hurryscan 14), which has mirrors and a focusing lens (f = 100 mm) that deliver the laser beams onto the target (powder bed) surface. The target surface is positioned at a certain vertical location where the laser spot diameters for the "sintering pulses" and the "pressing pulses" are both estimated to be ~180 μm via the knife-edge method and based on the approximate assumption of a Gaussian beam profile. As mentioned earlier, it is beyond the scope of this paper to study the achievable spatial resolution for DP-LMS, and hence relatively large laser spots are used to make it easier to observe the surface morphology of the sintered material lines. The nominal laser spot moving speed (achieved using the scan head or a motion stage not drawn in Fig.1a) on the powder bed surface is ~20 mm/s. The timing of the sintering and pressing laser pulses is controlled by the digital delay generator. Fig.1b shows the laser pulse format. In DP-LMS, each laser pulse group contains 10 "sintering pulses" fired at a pulse repetition rate of 25 kHz, followed by 1 "pressing pulse" at a delay time of τ_p (which is defined as the time interval

from the rising edge of the last preceding "sintering pulse" to the peak power moment of the "pressing pulse"). Then, after some time the next laser pulse group is fired, and the temporal interval between the rising edge of the last "sintering pulse" of the previous laser pulse group and the rising edge of the first "sintering pulse" of the next laser pulse group is τ_{gg}.

The cobalt powder used in this study has a nominal particle size of ~1.6 μm as listed in the specification of the product (Alfa Aesar, Product number: 10455). The powder spreading (coating) was achieved using a doctor blade. The powder was moisturized by ~95% ethanol before it was spread by the blade. Laser sintering was conducted in the ambient air after the powder dried. Typically, in each experiment the laser spots travel a path consisting of one or multiple straight-line sections to sinter a single-track surface layer, whose thickness is expected to be much smaller than the total thickness of the powder bed.

DP-LMS experiments (for single-track sintering) were conducted under various values of some major process parameters, such as the "pressing laser pulse" energy, delay time (τ_p), and the time interval between adjacent laser pulse groups (τ_{gg}). Sintering experiments were also performed using the "single pulse" format (i.e., only using the "sintering pulses" or the "pressing pulses" in each laser pulse group in Fig.1b). The sintered material lines were observed by an optical and/or scanning electron microscope (SEM) for surface morphology, material continuity, densification and possible defects such as pores and balling. The cross sections of some sintered samples were observed by SEM, and the surface elemental compositions of some cross sections were measured by energy-dispersive X-ray spectroscopy (EDS).

2.2 In-situ Time-resolved Temperature Measurements during DP-LMS and Related Principles

To help understand the underlying physical mechanism for some experimental results of laser sintering, in-situ time-resolved measurements of the powder bed surface temperatures were performed during DP-LMS. The measurement can provide the temperature history of a small measurement spot (which has approximately the same center location as, but is smaller than, the laser spots) on the powder bed surface during DP-LMS. Such temperature measurements are challenging due to the high spatial and temporal resolution requirements. They were performed based on a two-color pyrometry system set up by the authors to overcome the related challenges. The system determines the temperature by measuring target surface-emitted thermal radiation in two different wavelength ranges. It has the advantages of non-contact and not requiring the surface emissivity values. The reasonably high spatial resolution is achieved via an objective and a focusing lens in the system, while the reasonably high temporal resolution is facilitated by a photodetector with built-in amplifiers and ~ns scale rising time.

The schematic in Fig.1a also includes the two-color pyrometry system for the in-situ temperature measurement. It consists of an objective (Motic Plan APO ELWD 10x Microscope Objective, focal length: 20mm, numerical aperture (NA): 0.28), a beam splitter (Thorlabs BS015), a filter (either Type A or B), a focusing lens (Thorlabs LA1134-C, focal length: 60 mm), and an InGaAs photodetector (Thorlabs PDA015C/M; nominal detector size: Ø150 μm; the upper limit of the detectable wavelength range is ~1800 nm according to the product user guide). The optical axis of the pyrometry system has an angle of ~45^{o} relative to the powder bed surface. The system also includes a tube lens and a camera for the imaging required for the alignment purpose. The filter can be either Type A filter (longpass filter, Thorlabs FEL1200, cut-on wavelength: 1200 nm) or Type B filter (longpass filter, Thorlabs FEL1400, cut-on Wavelength: 1400 nm). When Type A filter is used, the system measures the thermal radiation emitted from the target surface in the

wavelength range of ~1200 to ~1800 nm. When Type B filter is used, it measures the thermal radiation in the range of ~1400 to 1800 nm. The photodetector converts the collected thermal radiation powder into a photocurrent, which eventually leads to a voltage signal that can be measured by an oscilloscope. The voltage signal histories (determined via a procedure introduced later) can be called $V_a(t)$ and $V_b(t)$ when Type A and B filters are used, respectively. Both Type A and B filters can block most of the laser light (if any) from entering the photodetector. In addition, during the temperature measurements for the results given in this paper it has been assumed that the thermal radiation power *emitted* by the powder bed surface that reaches the photodetector is much larger than that *reflected* by the surface, and the latter can be neglected.

Based on the setup, the measurement spot is approximately estimated to be an ellipse of ~50 × ~70 μm, whose center is approximately located at the laser spot center. Based on the NA of the objective lens, the thermal radiation emission from the measurement spot center within a cone (which has a half apex angle of ~16.26^o) can reach the photodetector. The measurement spot boundary is defined as the collection of the powder bed surface points whose thermal radiation emission within about half of such a cone can reach the photodetector. The measurement spot is reasonably small and the temperature variation with spatial locations within the spot has been approximately neglected. Hence, at a given moment one temperature is determined via the pyrometry system for the measurement spot. It has also been approximately assumed that under the conditions studied the surface spectral, directional emissivity, $\varepsilon(\lambda, T, \alpha, \beta)$, has a relatively weak wavelength dependence that can be approximately neglected, i.e., $\varepsilon(\lambda, T, \alpha, \beta) \cong \varepsilon(T, \alpha, \beta)$, in the wavelength range of 1200 to 1800 nm. The justification of this assumption will be discussed later.

Based on the assumptions above and the related thermal radiation theory [14], the ratio of the photodetector voltage signals can be given by:

$$\frac{V_a}{V_b} = \frac{\int\int_{\beta_1}^{\beta_2}\int_{\alpha_1}^{\alpha_2}\int_{1200\,nm}^{1800\,nm} Rs(\lambda)\varepsilon(\lambda,T,\alpha,\beta)I_b(\lambda,T)\sin(\alpha)\cos(\alpha)t_r(\lambda)\mathrm{d}\lambda\mathrm{d}\alpha\mathrm{d}\beta\mathrm{d}A}{\int\int_{\beta_1}^{\beta_2}\int_{\alpha_1}^{\alpha_2}\int_{1400\,nm}^{1800\,nm} Rs(\lambda)\varepsilon(\lambda,T,\alpha,\beta)I_b(\lambda,T)\sin(\alpha)\cos(\alpha)t_r(\lambda)\mathrm{d}\lambda\mathrm{d}\alpha\mathrm{d}\beta\mathrm{d}A}$$

$$= \frac{\int\int_{\beta_1}^{\beta_2}\int_{\alpha_1}^{\alpha_2} \varepsilon(T,\alpha,\beta)\sin(\alpha)\cos(\alpha)[\int_{1200\,nm}^{1800\,nm} Rs(\lambda)I_b(\lambda,T)t_r(\lambda)\mathrm{d}\lambda]\mathrm{d}\alpha\mathrm{d}\beta\mathrm{d}A}{\int\int_{\beta_1}^{\beta_2}\int_{\alpha_1}^{\alpha_2} \varepsilon(T,\alpha,\beta)\sin(\alpha)\cos(\alpha)[\int_{1400\,nm}^{1800\,nm} Rs(\lambda)I_b(\lambda,T)t(\lambda)\mathrm{d}\lambda]\mathrm{d}\alpha\mathrm{d}\beta\mathrm{d}A}$$

$$= \frac{\left[\int_{1200\,nm}^{1800\,nm} Rs(\lambda)I_b(\lambda,T)t_r(\lambda)d\lambda\right]\left[\int\int_{\beta_1}^{\beta_2}\int_{\alpha_1}^{\alpha_2} \varepsilon(T,\alpha,\beta)\,sin(\alpha)\,cos(\alpha)d\alpha d\beta dA\right]}{\left[\int_{1400\,nm}^{1800\,nm} Rs(\lambda)I_b(\lambda,T)t_r(\lambda)d\lambda\right]\left[\int\int_{\beta_1}^{\beta_2}\int_{\alpha_1}^{\alpha_2} \varepsilon(T,\alpha,\beta)\,sin(\alpha)\,cos(\alpha)d\alpha d\beta dA\right]}$$

$$= \frac{\int_{1200\,nm}^{1800\,nm} Rs(\lambda)I_b(\lambda,T)t_r(\lambda)d\lambda}{\int_{1400\,nm}^{1800\,nm} Rs(\lambda)I_b(\lambda,T)t_r(\lambda)d\lambda}$$

$$= \frac{\int_{1200\,nm}^{1800\,nm} Rs(\lambda)t_r(\lambda)\frac{2hc_0^2}{\lambda^5\left[\exp\left(\frac{hc_0}{\lambda k_b T}\right)-1\right]}\,d\lambda}{\int_{1400\,nm}^{1800\,nm} Rs(\lambda)t_r(\lambda)\frac{2hc_0^2}{\lambda^5\left[\exp\left(\frac{hc_0}{\lambda k_b T}\right)-1\right]}\,d\lambda} \qquad (1)$$

where dA denotes a differential area within the measurement spot, α_1, α_2, β_1 and β_2 define the solid angle range within which the thermal radiation emitted from a target surface point is detectable by the photodetector, $Rs(\lambda)$ is the photodetector responsivity (whose wavelength dependence is given in its user guide), $t_r(\lambda)$ is the total transmission of all the optical components that the thermal radiation emission passes through before reaching the photodetector (where the wavelength dependence of each component's transmission is available in the relevant product information from the corresponding vendor, except the objective lens, for which it has been assumed that the wavelength dependence of the transmission can be approximately neglected for the range of 1200 to 1800 nm), and $I_b(\lambda,T)$ denotes the spectral distribution of blackbody

emission. Based on the voltage signals $V_a(t)$ and $V_b(t)$, the measurement spot temperature can be determined via Eq.(1).

The following is the procedure to obtain $V_a(t)$ and $V_b(t)$ that will be put into Eq.(1) to deduce the temperature. For a given DP-LMS condition, N measurements are performed with Type B filter and Type A filter, respectively. The obtained photodetector voltage signal histories can be called, $U_{b,i}(t)$ and $U_{a,i}(t)$, respectively, where i = *1, 2, ... N*. Even in a dark environment, the photodetector can still produce a dark voltage signal with a mean voltage of $V_{dark,0}$ and a maximum oscillation amplitude of $V_{dark,amp}$. The mean dark voltage of the photodetector will be removed when the average voltage signal from N measurements is calculated:

$$V_{b,ave}(t) = [\frac{1}{N}\sum_{i=1}^{N} U_{b,i}(t)] - V_{dark,0} \qquad (2)$$

$$V_{a,ave}(t) = [\frac{1}{N}\sum_{i=1}^{N} U_{a,i}(t)] - V_{dark,0} \qquad (3)$$

Then, to decrease high-frequency noise, the signals, $V_{b,ave}(t)$ and $V_{a,ave}(t)$, are processed by a Butterworth low-pass filter in Matlab (5th order; normalized cutoff frequency: 0.0121; normalization is based on the oscilloscope sampling frequency of 25 MHz) to get $V_{b,ave\_f}(t)$ and $V_{a,ave\_f}(t)$, respectively. For the signal curve $V_{b,ave\_f}(t)$ versus t, its portion below $2V_{dark,amp}$ is truncated (because this portion is not significantly larger than the dark voltage oscillation amplitude and could be un-reliable for the temperature deduction), and the resulted signal will be called $V_b(t)$. Then $V_{a,ave\_f}(t)$ is truncated to obtain $V_a(t)$. The truncation is performed in a way to make $V_a(t)$ have the same duration as $V_b(t)$. Based on the obtained $V_a(t)$ and $V_b(t)$ signals, the measured temperature history $T(t)$ can be deduced via Eq.(1).

Finally, the previously mentioned assumption about the weak wavelength dependence of the emissivity in the range of 1200 to 1800 nm will be discussed. Based on the Kirchhoff's law [14], the surface spectral, directional emissivity, $\varepsilon(\lambda, T, \alpha, \beta)$, can be determined as one minus the

surface spectral, directional reflectivity. The surface reflectivity can be estimated via the Fresnel equations [15] based on the target material complex index of refraction (which is an intrinsic material optical property). The index of refraction can be estimated via the Drude model [15-17] based on the target metal plasma frequency and the DC electrical conductivity. Ref. [17] lists a constant value of the cobalt plasma frequency (more related details are given in [17]). Refs.[18] lists the solid and molten cobalt electrical conductivities at different temperatures. Based on these, the emissivity variation with the wavelength in the range of 1200 to 1800 nm is estimated via the Drude model and Fresnel equations for the following conditions: solid cobalt at 1400 K, solid cobalt 1767 K, liquid cobalt at 1767 K, liquid cobalt at 2300 K, 2600 K and 3000 K for the incidence angle of 45^o, 45^o+16^o, and 45^o-16^o, respectively, for both the transverse electric (TE) and transverse magnetic (TM) situations. The measured temperatures in this paper and the involved emissivity angles are mostly within these ranges. For all the calculated conditions, it has been found that the emissivity variation with the wavelength is small in the range of 1200 to 1800 nm. Although the theoretical analysis is very approximate, it should provide a reasonable support for the approximate assumption that the wavelength dependence of the emissivity can be neglected for the range of 1200 to 1800 nm.

For in-situ temperature measurements, the powder bed surface is moved by a motion stage, while the laser beam and the pyrometry system (hence its measurement spot) stay stationary relative to the laboratory ground. Hence, the relative location between the laser spots and the measurement spot stays the same. For laser sintering experiments without in-situ temperature measurements, the relative motion of the laser spots on the powder bed surface is achieved either by moving the powder bed with a motion stage or by moving the laser spots with the scanhead. In the authors' previous work [19], a similar two-color pyrometry approach was used to measure the

target surface temperature during single-beam laser sintering of carbon nanotube-silver composite thin films on a polymer substrate, and the study in [19] was not for DP-LMS. Ref.[19] shows that under the irradiation by a train of laser pulses, the target surface melting duration deduced from the temperature measurement with the two-color pyrometry approach agrees well with that deduced via the surface-reflected probe laser light measurement. This has provided a verification of the validity of the temperature measurement approach.

3. Results and Discussions

3.1 Experimental Results on Laser Sintering

Figure 2 shows optical microscopic images for the sintering results by DP-LMS and those by only using the "sintering pulses" (without the "pressing pulse") in Fig. 1b. Fig.2c shows the material lines (which form a near-rectangular shape) sintered by only using the "sintering pulses" with an average pulse energy of ~0.067 mJ. Severe balling can be observed and the sintered material do not appear to be very continuous or densified. On the other hand, Fig.2a shows the material lines sintered by DP-LMS, and the condition differs from that in Fig.2c. In Fig.2a, an additional "pressing laser pulse" with the pulse energy of ~0.179 mJ is used for each laser pulse group. The sintered lines show much less severe balling and appear to be much more continuous and densified than those in Fig.2c. The central regions of the lines in Fig.2a also appear more shiny overall, which likely implies better surface smoothness. Is the better sintering result in Fig.2a than that in Fig.2c simply due to more laser pulse energy input in each pulse group? The answer should be No as implied by Fig.2e, which shows the sintered lines by only using "sintering pulses", but with a higher average pulse energy of ~0.084 mJ (such that the total laser energy per laser pulse group is very close to that for DP-LMS in Fig.2a). However, the sintered lines still show severe

balling and overall the ball sizes appear to be larger than those in Fig.2c. The sintered material still appears to be much less densified or continuous than that in Fig.2a. Figs.2b, 2d and 2f show optical microscopic images of a portion of the sintered lines in Figs.2a, 2c and 2e, respectively. They show the aforementioned corresponding characteristics more clearly.

Figure 3a and 3c show the SEM images of a material line sintered by DP-LMS and by only using the "sintering pulses", respectively. Fig.3c shows that the sintered line mainly consists of many spherical or near-spherical balls. Due to the severe balling phenomenon, the medium is very porous and appears to have poor densification. In contrast, Fig.3a shows that the line sintered by DP-LMS exhibits much less severe balling, much lower porosity and overall appears to be much more continuous and densified than that in Fig.3c. There is only a much smaller number of balls near the line boundary in Fig.3a. Fig.3b and 3d show SEM images at a higher magnification for a region sintered by DP-LMS and that by only using the "sintering pulses", respectively. The images show more clearly that the metal medium sintered by DP-LMS appear to be much more continuous and densified. One thing observed related to the balling phenomenon for laser sintering only using the "sintering pulses" is that higher laser pulse fluence appears to produce larger balls overall, which can be seen by comparing Fig.2d with 2f. This can also be seen from the SEM image in Fig.3c, where the ball size in the line central region (where the local laser fluence is larger) appears to be overall larger than that near the line boundary region. Figure 3e and 3f show the SEM images of a material line sintered by only using the "pressing pulses". The "pressing laser pulse" energy per pulse is the same as that in the DP-LMS process for Fig.3a. Under the condition given, the sintered regions in the SEM images in Fig.3e and f appear obviously more porous than those in Fig.3a and 3b for the DP-LMS process.

Figure 4 shows cross-sectional SEM images for material lines sintered by DP-LMS (the top row) and SP-LMS with "sintering pulses" alone (the bottom row), respectively. In Fig.4a, a reasonably continuous sintered layer can be clearly seen, below which are the un-sintered cobalt powders. A higher-magnified SEM image of a portion of the region in Fig.4a is shown in Fig.4b, in which the sintered region material appears very densified. In Fig.4c, the cross section of the sample sintered by SP-LMS with "sintering pulses" alone shows large and separate balls or blocks. The morphology is consistent with the severe balling phenomenon observed in the top-surface SEM images in Fig.3c and d for a material line sintered by SP-LMS with only the "sintering pulses". The sintered region (i.e., the region with relatively large balls and/or blocks) in the cross-section in Fig.4c appears much less continuous than that in Fig.4a. It should be noted that the width of the sintered layer by DP-LMS is much larger than its thickness, and thus the layer might be easily deformed during the sample mounting process, which could be a reason (or one of the reasons) for the layer deformation observed in the SEM image in Fig.4a.

Figure 5a and 5b show the elemental composition maps obtained via EDS measurements for cross-sectional regions of samples sintered by DP-LMS and by SP-LMS with only the "sintering pulses", respectively. Figure 5c shows the weight percentages of elements for the measured regions in (a) and (b). It can be seen that the elemental map and weight percentages for the sample by DP-LMS are similar to those for the sample by SP-LMS. For the regions of both maps, the EDS results show that the cobalt element dominates in the cross section, and the oxygen percentage is very low. This implies that the cobalt element likely dominates in the *bulk* of the sintered material. Thus, for the purpose of the study in this paper, it is sufficient to perform the sintering in the ambient air. On the other hand, EDS measurements were also performed on a DP-LMS sample *top* surface, which show that a significant amount of oxygen element does exist on

the top surface. Hence, for situations where the top surface oxidation needs to be minimized, the sintering can be performed in an inert gas environment. The cobalt powder used in the sintering has a high purity based on the product specification from the vendor. Hence, it is expected that the carbon element shown in the EDS results in Fig.5 should be mainly due to the carbon contamination of the EDS sample surface, which is a common phenomenon in EDS measurements and does not affect the purpose of the EDS measurement in this paper.

Figure 6 shows optical microscopic images of material lines sintered by DP-LMS with different delay time for the "pressing laser pulse" in each laser pulse group (τ_p = 25 μs, 125 μs and 625 μs for Fig.6a, 6b and 6c, respectively). The morphologies obtained with τ_p = 25 μs and 125 μs are similar to each other. However, for τ_p = 625 μs, Fig.6c shows that the sintered material exhibits more obvious balling and appears to be less densified and/or continuous.

Figure 7a and 7b show optical microscopic images of lines sintered by DP-LMS with different "pressing laser pulse" energies of ~0.138 and ~0.179 mJ, respectively. The sintered line in Fig.7b appears to be reasonably dense and continuous. However, the sintered line in Fig.7a appears to be more porous and less continuous. The results in Figs.6 and 7 imply that in DP-LMS the "pressing laser pulse" needs to be fired at suitable timing with a sufficient high pulse energy to obtain good sintering results.

Figure 7c shows the electrical resistance of ~14-mm material lines sintered by DP-LMS with the pressing pulse energy of ~0.138 mJ or ~0.179 mJ per pulse (i.e., with major laser parameters the same as those in Fig.7a and b, respectively). The resistance is measured via the four-point probe method. Microscopic observations suggest that the sintered line cross-sectional areas do not differ very significantly with the two different "pressing pulse" energies. Hence, the much lower average electrical resistance of the lines sintered with the "pressing pulse" energy of

~0.179 mJ/pulse should indicate obviously better coalition and/or continuity of the material sintered in this condition than that with the smaller "pressing pulse" energy of ~0.138 mJ/pulse. This comparison result is consistent with the surface morphology indicated by the micrographs in Fig.7a and 7b, which show that the material sintered with the "pressing pulse" energy of ~0.179 mJ appears more continuous and densified. This also provides support that the sintered region surface morphology shown in the micrographs in this paper, although qualitative in nature, is expected to be an acceptable quality indicator for the purpose of the study in this paper. Hence, the sintering quality comparisons in this paper are mainly based on the morphologies in the micrographs. For Fig.7c, the "pressing laser pulse" delay time in DP-LMS is 125 μs. Under the conditions studied, the samples sintered by SP-LMS with only the "sintering laser pulses" and the samples sintered by DP-LMS with a too long "pressing laser pulse" delay time of 625 μs (i.e., with major laser parameters the same as those for Fig.6c) are often so fragile that it is difficult to reliably measure their resistance. The sample fragility is a further indication that the sintering results under these conditions are worse than those by DP-LMS with the laser conditions for Fig.7c.

Figure 8 shows optical microscopic images of lines sintered by DP-LMS with different temporal distances between adjacent laser pulse groups, where τ_{gg} = 640 μs, 1040 μs and 1440 μs for Fig.8a, 8b and 8c, respectively. A very interesting phenomenon is observed. The sintered line in Fig.8b appears to be more continuous and less porous than those in Fig.8a and 8c. In other words, under the conditions studied, if the group-to-group temporal distance is too large or too small, it is not beneficial for the sintered material densification.

In a short summary, Figs. 2-4, 6-8 show that under the conditions studied: (1) DP-LMS can produce sintered material lines that appear to be much more continuous and densified with much less severe balling than those by LMS under similar conditions but only using the "sintering

pulses" without the "pressing pulse" in each pulse group. (2) In DP-LMS a "pressing laser pulse" with a sufficiently high pulse energy needs to be fired at a time sufficiently close to the last "sintering laser pulse" in the same pulse group to get good sintering results. (3) In DP-LMS, the temporal distance between adjacent pulse groups should not be too large or too small. The possible underlying fundamental mechanisms for these observations will be analyzed and discussed in the next two sections.

3.2 Fundamental Mechanism Analysis for Different Results by DP-LMS and SP-LMS with Only the "Sintering Pulses"

The authors' previous paper [13] has briefly discussed the possible fundamental mechanism for DP-LMS. In this paper, this section explains the expected fundamental mechanism in more details for the different sintering results obtained by DP-LMS and by single-pulse LMS (SP-LMS) with only the "sintering pulses" under the conditions studied. The mechanism is demonstrated in Fig.9. Future work may still be needed to further verify the proposed fundamental mechanism.

The powder apparent density in the powder bed in this study (which was approximately estimated by measuring the powder weight and apparent volume) is only ~28% of the bulk cobalt [20]. The nominal particle size is very small (only ~1.6 μm based on the product specification). The particle surface-to-volume ratio is high, which makes the ratio of the inter-particle surface force to the gravity force high, and the particles tend to agglomerate into many clusters. Under the irradiation of the "sintering laser pulses", the particle melting (or partial melting) and/or coalition may occur. Then, driven by surface tension, some molten material could contract into many

individual balls. A larger laser fluence may yield more severe coalition and overall larger ball sizes.

For single-pulse LMS with only the "sintering pulses", the aforementioned molten metal balls will cool down and re-solidify. As a result, the sintered medium may exhibit severe balling and have poor densification as shown in Figs.2(c-f) and 3(c, d).

On the other hand, for DP-LMS, in each laser pulse group a "pressing laser pulse" is fired to the powder bed material surface ("target surface"). Compared with the "sintering pulses", the "pressing pulse" has a much shorter duration of ~4 ns (vs. ~200 ns for each "sintering pulse") and a much higher transient intensity. The "pressing laser pulse" may ablate a small amount of the material and generate a high-pressure plasma plume, which can induce a high transient pressure onto the target surface [6, 21, 22]. This may promote the melt flow and help transform many molten balls into a more continuous and flat molten layer, which then re-solidifies into a more continuous and densified solid layer with much less severe balling as shown in Figs.2(a, b) and 3(a, b). As shown later, the in-situ temperature measurement results are consistent with, and hence provide supporting evidence to, this expected fundamental mechanism.

3.3 Fundamental Mechanism Analysis for Parameters' Effects in DP-LMS

Figs.6 to 8 suggest the following parametric effects in DP-LMS under the conditions studied, that is, in order to obtain good sintering results:

Effect (1): with a given laser pulse duration and spot size, the "pressing pulse" energy needs to be sufficiently high (as implied by Fig.7);

Effect (2): the "pressing pulse" needs to follow the last "sintering pulse" in the same group close enough (as implied by Fig.6);

Effect (3): the temporal distance between adjacent pulse groups needs to be suitable (not too large or too small) under the given laser spot moving speed on the powder bed surface (as implied by Fig.8).

Effect (1) seems to be easy to understand. The "pressing laser pulse" needs to have a sufficiently high transient intensity (i.e., sufficiently high pulse energy with a given pulse duration and spot size) in order to produce sufficiently high transient pressures via laser ablation plasma.

Effect (2) will be discussed next based on in-situ time-resolved temperature measurement results during DP-LMS shown in Fig.10a and 10b, where the major laser parameters are the same as those for Fig.6b and 6c, respectively. In the DP-LMS process for Fig.10a, each laser pulse group has 10 "sintering pulses" (with a pulse-to-pulse time interval of 40 μs) followed by 1 "pressing pulse" at a delay time of τ_p = 125 μs. For Fig.10b, the delay time is τ_p = 625 μs.

Fig.10a shows 10 temperature oscillation peaks, which are induced by the 10 "sintering pulses" in a laser pulse group. The peak-to-peak temporal distance is around 40 μs, similar to the temporal distance between adjacent "sintering pulses". The figure shows the temperature history until the moment slightly before the "pressing pulse" is fired. It can be seen that at this moment, the measurement spot temperature is still well above the melting point [20]. Hence, the surface material in the measurement spot is still substantially in a molten state. Because the laser spot and the measurement spot have about the same center location, it is expected that the "pressing laser pulse" can induce high pressures onto the molten metal surface, promoting melt flow, reducing balling and/or enhancing densification and/or continuity. Hence, a reasonably good sintering result is shown in the micrograph in Fig.6b, where the DP-LMS process is performed with major laser parameters the same as those for Fig.10a. The measurement spot temperature history after the "pressing pulse" irradiates the surface is not shown, because the "pressing laser pulse" generates

plasma, the emitted radiation of which will also reach the photodetector in the pyrometry system in Fig.1a and could overwhelm the thermal radiation emitted from the measurement spot when the plasma radiation is strong.

Fig.10b shows the measured temperature history until the moment slightly before the "pressing laser pulse" is fired, which comes at a delay time of τ_p = 625 μs (500 μs longer than that for Fig.10a). It can be seen that at this moment, the measurement spot temperature is already lower than the melting point of cobalt. Hence, the irradiated surface region by the "pressing laser pulse" has already solidified (or mostly solidified). It is expected that this will greatly weaken the aforementioned beneficial effect of the "pressing laser pulse". Because the major laser parameters for Fig.10b are the same as those for Fig.6c, this provides a fundamental explanation about why the sintered region shown in the micrograph in Fig.6c appears much less continuous and densified (with more obvious balling) than that in Fig.6b.

The temperature measurement results in Fig.10 have helped reveal the underlying physical mechanisms for the different sintering results by DP-LMS with different "pressing laser pulse" delay time. In addition, the results clearly show the thermal accumulation effect between adjacent "sintering laser pulses" under the conditions studied. After one "sintering laser pulse", the surface material (in the measurement spot) is still at an obviously elevated temperature when the next "sintering laser pulse" comes. This implies that all the "sintering pulses" in a pulse group, not just the last one, could influence the surface temperature when the "pressing laser pulse" is fired.

The main purpose of the temperature measurements in this paper is to help understand the effect of the different "pressing laser pulse" delay time under the conditions studied, and hence the measurement spot temperature at around one to a few hundred μs after the last "sintering pulse" is of major interest. A Butterworth low-pass filter was used to reduce high-frequency noise of the

photodetector signals in the measurements. The selected oscilloscope sampling frequency and the Butterworth filter parameters (as described earlier) should be able to satisfy the aforementioned purpose sufficiently well, although they may reduce the slope and degrade the temporal resolution of the ten rising edges in each temperature history curve in Fig.10 (and also slightly affect the ten falling edges and the magnitudes of the ten local peaks). In each of the DP-LMS experiments for Fig.10, the powder bed surface was moved by a motion stage at ~20 mm/s and a total of ~571 laser pulse groups were fired. The temperature measurement was conducted for approximately the middle laser pulse group.

Effect (3) is a very interesting effect. Figure 8c shows that when the temporal distance between adjacent pulse groups is too long, the sintered material appears to be overall less continuous. It is expected that this should be related to the less laser energy input per unit area under the longer group-to-group temporal distance (with a given laser spot moving speed). On the other hand, Fig.8a shows that when the group-to-group temporal distance is too short, the sintered material appears to be more porous and exhibits more severe balling. The following is the expected mechanism. When the group-to-group temporal distance is very short, due to the potential group-to-group thermal accumulation effect, the "sintering laser pulses"-induced melt pool size and/or molten metal amount may become too large. Hence, the pressure impact (the impact magnitude and/or impacted region size) due to the "pressing laser pulse" may become insufficient in transforming the molten metal balls into a more continuous and flat metal layer. This may lead to a less continuous sintered medium with more obvious balling as shown in Fig.8a.

The proposed fundamental mechanisms in Section 3.2 and 3.3 of this paper may still require future work to further confirm and verify.

As mentioned earlier, relatively large laser spots were used in this study to make it easier to observe the surface morphology of the sintered material lines. It is beyond the scope of this paper to study the achievable spatial resolution for DP-LMS. Due to the small particle sizes and short pulse durations that can be used, it is expected that a good spatial resolution is potentially achievable by DP-LMS. The sintering in this paper is still called "micro" sintering because the used particle size is on the order of ~1 μm, which is much smaller than the typical particle sizes for the conventional macro-scale selective laser sintering or melting. Such a small particle size can potentially make it possible to sinter very small micro features, and meanwhile it can often make it challenging to obtain good densification and/or continuity for sintered material as introduced earlier.

3.4 Advantages of DP-LMS and General Guidelines on Parameter Selection

The advantages of DP-LMS and its general parameter selection criteria were briefly discussed in the authors' previous paper [13]. These will be discussed in more details in this paper.

Under the conditions studied in this paper, DP-LMS shows better sintering results than those by SP-LMS only using sintering or pressing pulses. The major concept of DP-LMS is to use two types of pulses to achieve the purpose of "sintering" and "pressing", respectively. It is possible to do both "sintering" and "pressing" with just one type of laser pulses at sufficiently high intensities. However, using two types of laser pulses, as in DP-LMS, offers the potential advantages of much better flexibility, adjustability and/or controllability. The parameters of the "sintering pulse(s)" and those of the "pressing pulse(s)" in each pulse group can be selected for the purpose of "sintering" (i.e., generating sufficient powder melting with no or little ablation) and for the purpose of "pressing" (i.e., generating sufficiently high pressures via ablation, but without

removing too much material), *respectively*. For each laser pulse group, the amount and temperature of molten metal generated can be adjusted by changing the parameters of the "sintering laser pulse(s)" without significantly affecting the subsequent pressures induced by the "pressing laser pulse(s)" on the surface. The pressures exerted on the surface can be adjusted by changing the parameters of the "pressing laser pulse(s)". The moment of the pressure impact onto the powder bed surface can be adjusted by changing the delay time of the "pressing laser pulse(s)". In a broad sense, a SP-LMS process with the "sintering" or "pressing" pulses alone is just a special sub-set of the DP-LMS process. In this sense, the best achievable result by a DP-LMS system can only be better than (or at least the same as) that by a SP-LMS system equipped with only one of the two lasers in the DP-LMS system, and the DP-LMS system could offer much better process adjustability, flexibility and/or controllability. It should also be noted that the equipment cost of an additional suitable nanosecond laser is typically much lower than the total cost of a complete commercial selective laser sintering or melting system [23].

Finally, a general parameter-selection guideline for DP-LMS is given. Typically, the parameters of "sintering laser pulses" should be suitably selected for the purpose of "sintering" (i.e., generating sufficient particle melting with little material removal by ablation). Typically, a reasonably long pulse duration for the "sintering pulses" (e.g., on the scale of ~100 ns) may be desirable to facilitate the generation of sufficient melting. The fluence(s) of the "sintering pulse(s)" in each pulse group (considering the possible pulse-to-pulse thermal accumulation effect) should be higher than the powder bed melting threshold, but lower than (or at least not obviously higher than) its ablation threshold. On the other hand, typically the parameters of the "pressing laser pulses" should be suitably selected for the purpose of "pressing" (i.e., generating a sufficiently high pressure pulse onto the powder bed surface by ablating a small amount of material). Typically,

the laser-induced transient peak pressure increases with the laser pulse peak power density (I, unit: W/cm^2), while the amount of material ablated per unit surface area increases with the laser pulse fluence (F, unit: J/cm^2). Hence, the "pressing laser pulse" should have a sufficiently high peak power density, but not a too high fluence. Therefore, it should also have a relatively short pulse duration (τ, which is typically proportional to F/I), e.g., on the scale of a few ns. Typically, the "pressing laser pulse" should be fired when the irradiated surface region is still in a molten state (or partially so to a sufficient extent), so that its induced pressure can help promote molten metal flow, reduce balling and/or enhance densification and/or continuity. DP-LMS is a novel technology that is still being studied. Hence, the general guideline above is subject to possible future modifications and/or improvements.

4 Conclusions

This paper reports single-track experimental study of a novel double-pulse laser micro sintering (DP-LMS) process previously proposed by the corresponding author [12], and the related fundamental mechanism analysis with the help of in-situ time-resolved temperature measurements via a two-color pyrometry system. The studied DP-LMS process utilizes laser pulse group(s), each of which consists of two types of laser pulses: ten low-intensity, long-duration "sintering laser pulses", and one high-intensity, short-duration "pressing laser pulse". Under the conditions investigated, the following has been found:

(1) In an ambient air environment, the novel DP-LMS process can produce material lines that appear to be more densified and/or continuous than those by single-pulse laser micro sintering with only the sintering or pressing pulses.

(2) The fundamental mechanism for the better sintering results by **DP**-LMS compared to **SP**-LMS with only the "sintering pulses" is expected to be the following: under the irradiation by "sintering laser pulses", the melted particles tend to contract into individual balls due to surface tension. Compared to SP-LMS, the additional high-intensity "pressing laser pulse" in each pulse group in DP-LMS can ablate a small amount of material and generate a plasma plume, which can induce a high transient pressure onto the powder bed surface to promote molten metal flow, reduce balling and/or enhance densification and/or continuity.

(3) In order for the "pressing laser pulse" to be effective, its intensity (and hence pulse energy under the given laser pulse duration and spot size) needs to be sufficiently high to produce a sufficiently high pressure. It also needs to follow the "sintering pulses" closely enough in time. As revealed by the in-situ temperature measurements, a "pressing pulse" fired when the irradiated surface region is still in a molten state (or partially so to a sufficient extent) produces much better material continuity and/or densification than that fired when the surface region has mostly solidified. This is consistent with, and provides supporting evidence for, the aforementioned DP-LMS fundamental mechanism.

(4) The in-situ temperature measurements suggest that a thermal accumulation effect exists between adjacent "sintering laser pulses" in each pulse group, where the surface region irradiated by one "sintering laser pulse" is still at an elevated temperature when the following "sintering laser pulse" comes.

(5) To obtain a good sintering result in DP-LMS, the laser pulse group-to-group temporal distance needs to be sufficiently small to ensure sufficient energy input per unit area under a given laser spot traveling speed. On the other hand, the inter-group distance needs to be sufficiently large to avoid generating a melt pool (and/or molten material amount) that is too large for the

"pressing laser pulse" to effectively impact. This is expected to be the fundamental mechanism for the observed parametric effect of the inter-group temporal distance.

To the authors' knowledge, DP-LMS is a novel process proposed in a recent year that is still under study. The sintering results presented in this paper do not necessarily represent the best possible results under the given setups. Further work is still needed to better understand the manufacturing performance and the fundamental mechanisms of DP-LMS. In particular, it could be good work in the future to perform further microstructure characterizations for DP-LMS.

Acknowledgment and Declaration of Interest

This material is based upon work supported by the National Science Foundation under Grant No. CMMI 1728481. The grantee organization is Purdue University (West Lafayette, IN). The corresponding author is the inventor of a filed patent application on DP-LMS [12].

List of References

1. Kruth, J.P., Mercelis, P., Van Vaerenbergh, J., Froyen, L., Rombouts, M., “Binding mechanisms in selective laser sintering and selective laser melting”, Rapid Prototyping Journal, 11: 26-36, 2005.
2. Wang, Y., Shi, J., Lu, S. and Wang, Y., “Selective laser melting of graphene-reinforced Inconel 718 superalloy: evaluation of microstructure and tensile performance”, Journal of Manufacturing Science and Engineering, 139: 041005, 2017.
3. Guo, N., Leu, M.C., “Additive manufacturing: technology, applications and research needs”, Frontiers of Mechanical Engineering, 8: 215–243, 2013.
4. Ko, S. H., Pan, H., Grigoropoulos, C. P., Luscombe, C. K., Fréchet, J. M. J., Poulikakos, D., “All-inkjet-printed flexible electronics fabrication on a polymer substrate by low-temperature high-resolution selective laser sintering of metal nanoparticles”, Nanotechnology, 18: 345202, 2007.
5. Lin, D., Liu, C.R., Cheng, G.J., "Laser sintering of separated and uniformly distributed multiwall carbon nanotubes integrated iron nanocomposites." Journal of Applied Physics 115: 113513, 2014.
6. Regenfuss, P., Streek, A., Hartwig, L., Klötzer, S., Brabant, Th., Horn, M., Ebert, R., Exner, H., "Principles of laser micro sintering", Rapid Prototyping Journal, 13:204-212, 2007.
7. Streek, A., Regenfuss, P., Exner, H., "Fundamentals of energy conversion and dissipation in powder layers during laser micro sintering", Physics Procedia, 41:851–862, 2013.
8. Zhu, H., Ke, L., Lei, W., Dai, C., Chen, B., "Effect of the Q-switch parameters on the sintering behavior of laser micro sintering Cu-based metal powder using Q-switched Nd-YAG laser." Rapid Prototyping Journal, 19: 44-50, 2013.
9. Ke, L., Zhu, H., Yin, J., Wang, X., "Effects of peak laser power on laser micro sintering of nickel powder by pulsed Nd: YAG laser." Rapid Prototyping Journal, 20: 328-335, 2014.
10. Streek, A., Regenfuss, P., Ebert, R., Exner, H., "Laser micro sintering–a quality leap through improvement of powder packing", 2008 International Solid Freeform Fabrication Symposium.
11. Vaezi, M., Seitz, H., Yang, S., "A review on 3D micro-additive manufacturing technologies", The International Journal of Advanced Manufacturing Technology, 67:1721-1754, 2013.
12. Wu B, inventor; Purdue Research Foundation, assignee. *Processes and systems for double-pulse laser micro sintering*. United States patent application. Application Number: 16/427,638, filed on 5/31/2019 (related provisional patent application number: 62693684, filed on 07/03/2018).
13. Song, H., Kang, Z., Liu, Z., Wu, B., “Experimental study of double-pulse laser micro sintering: A novel laser micro sintering process”, Manufacturing Letters, 19:10-14, 2019.
14. Incropera, F.P., DeWitt, D.P., Fundamentals of Heat and Mass Transfer. John Wiley & Sons, 2002.
15. Pedrotti, F. L., Pedrotti, L. S., Pedrotti, L.M., Introduction to Optics. Pearson Prentice Hall, 2007.

16. Li, H.Y., Zhou, S.M., Li, J., Chen, Y.L., Wang, S.Y., Shen, Z.C., Chen, L.Y., Liu, H., Zhang, X.X., 2001. “Analysis of the Drude model in metallic films”, Applied Optics, 40(34): 6307-6311, 2001.
17. Ordal, M.A., Bell, R.J., Alexander, R.W., Long, L.L., Querry, M.R., “Optical properties of fourteen metals in the infrared and far infrared: Al, Co, Cu, Au, Fe, Pb, Mo, Ni, Pd, Pt, Ag, Ti, V, and W”, Applied Optics, 24(24): 4493-4499, 1985.
18. Chu, T.K. and Ho, C.Y. Electrical Resistivity of Chromium, Cobalt, Iron, and Nickel. CINDAS Report 60, June 1982.
19. Song, H, Kang, Z., Wu, B., “Time-resolved in-situ temperature measurement and analysis for continuous-wave laser sintering of carbon nanotube – metal composites on a polymer substrate”, Journal of Manufacturing Processes, 66: 435-445, 2021.
20. Fleitman, A.H., Herchenroeder, R.B., Chow, J.G.Y, “Cobalt-base alloys for use in nuclear reactors”, Nuclear Engineering and Design, 15:345-62, 1971.
21. Tao, S., Zhou, Y., Wu, B., Gao, Y., “Infrared long nanosecond laser pulse ablation of silicon: integrated two-dimensional modeling and time-resolved experimental study”, Applied Surface Science, 258:7766–7773, 2012.
22. Zhou, Y., Tao, S., Wu, B., “Backward growth of plasma induced by long nanosecond laser pulse ablation”, Applied Physics Letters, 99(5): 051106, 2011.
23. https://www.fabbaloo.com/blog/2017/6/2/a-look-inside-slm-solutions-new-3d-metal-printers (last accessed on April 8, 2021).

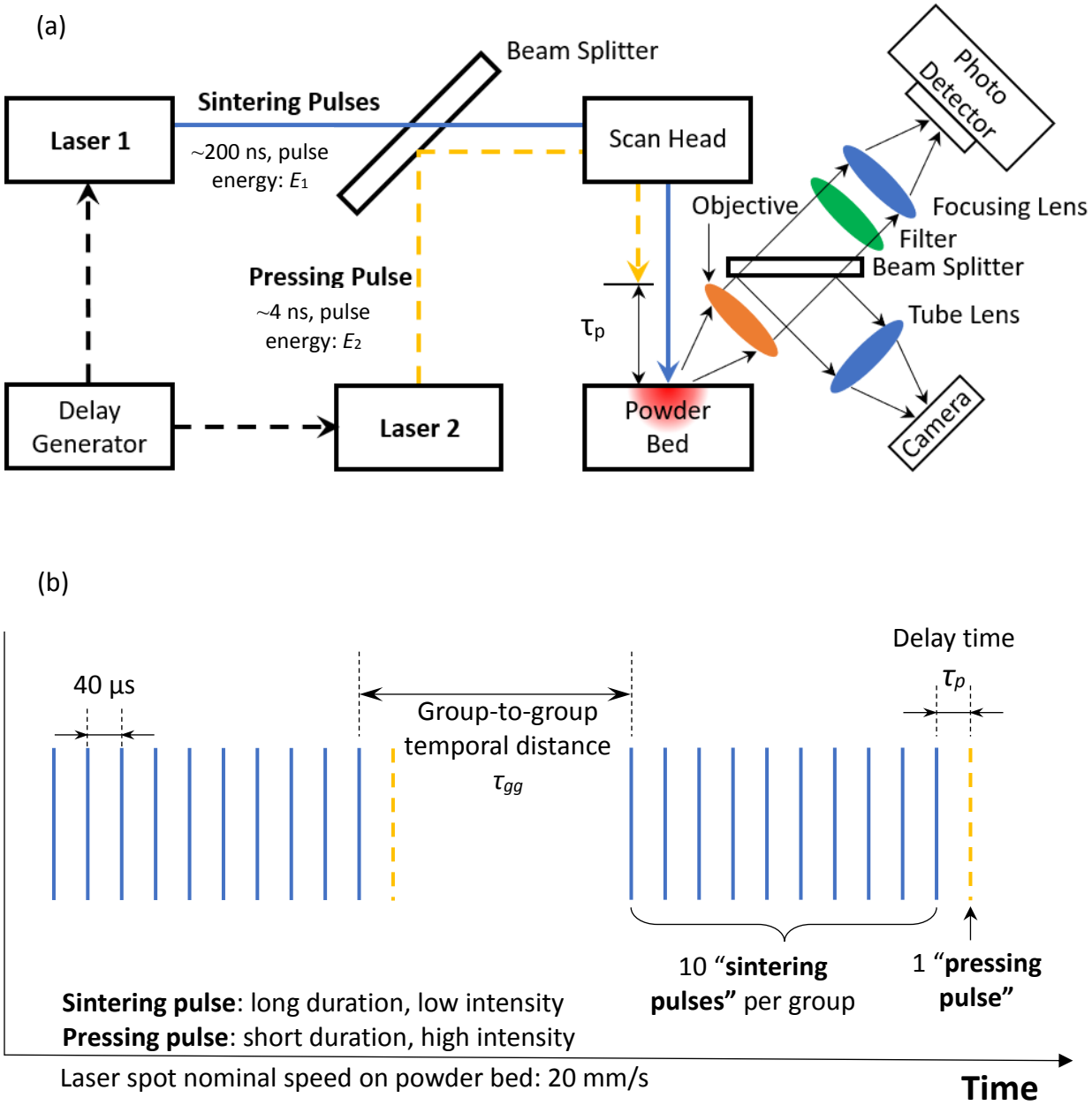

Figure 1. Schematic diagrams for: (a) the experimental setup for double-pulse laser micro sintering (DP-LMS) including the pyrometry system for in-situ temperature measurements (showing only some major components); (b) the laser pulse format employed for the DP-LMS process in this study (which only shows the pulse timing, not the pulse power, duration or temporal profile).

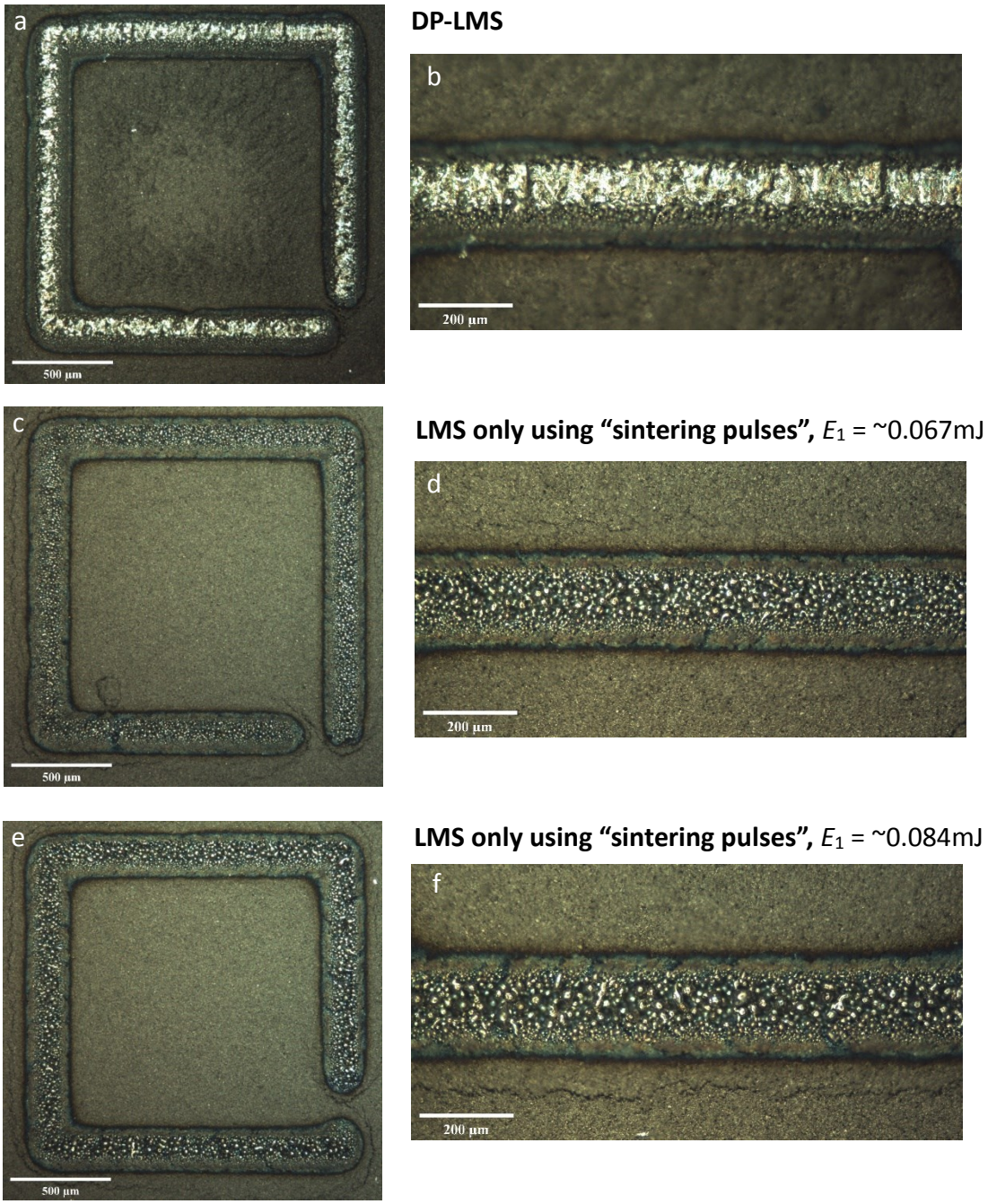

Figure 2. Optical microscopic images of powder bed surface regions sintered by: (a)(b) DP-LMS (average "sintering laser pulse" energy E_1 = ~0.067 mJ per pulse, "pressing laser pulse" energy E_2 = ~0.179mJ, "pressing laser pulse" delay time τ_p = 125 µs); (c)(d) LMS only using the "sintering pulses" (E_1 = ~0.067mJ); (e)(f) LMS only using "the sintering pulses" with a higher average pulse energy (E_1 = ~0.084mJ) (for (a) to (f), adjacent pulse group temporal distance τ_{gg} = 1040 µs).

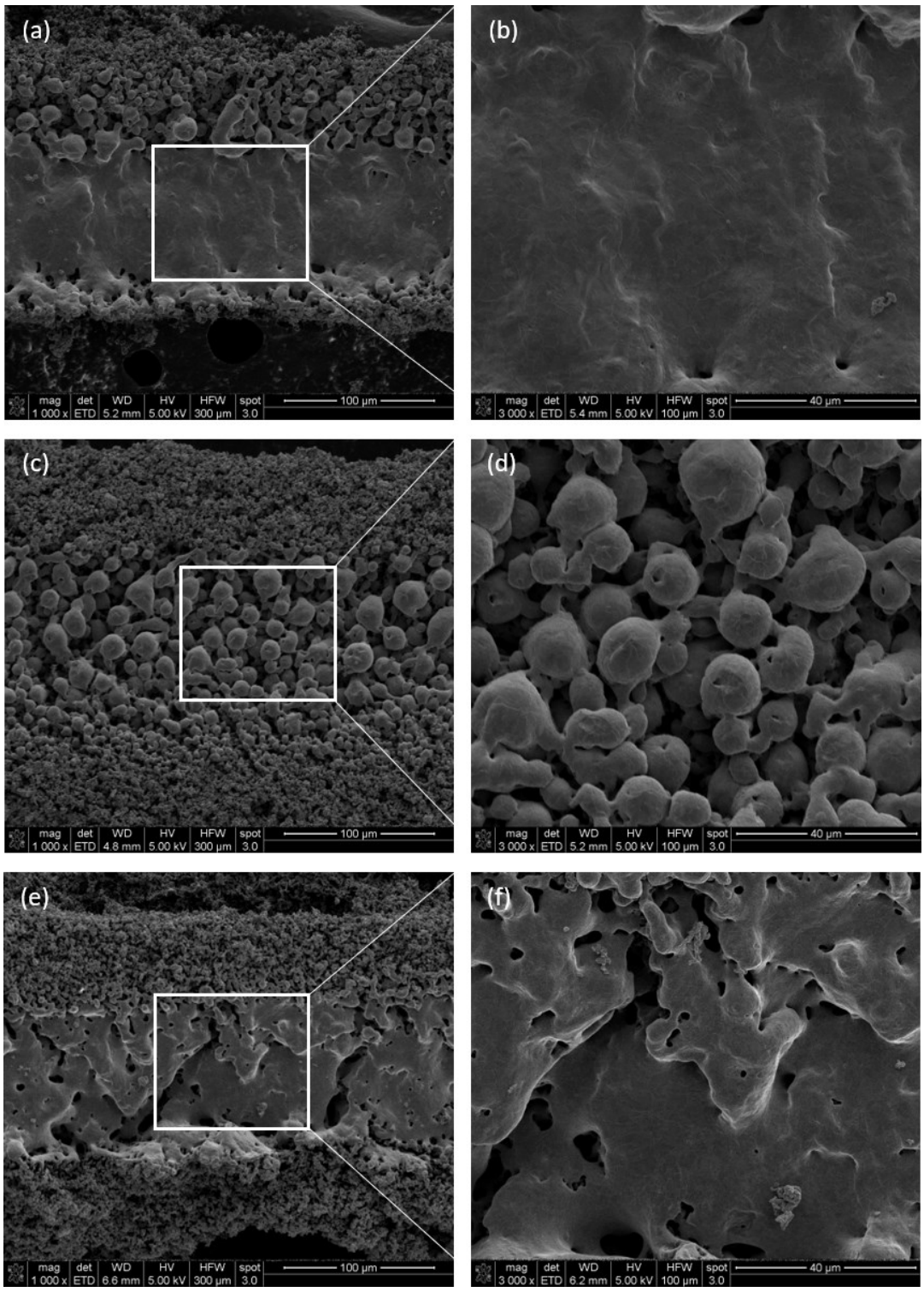

Figure 3. SEM images showing a surface region sintered by: (a)(b) DP-LMS, (c)(d) SP-LMS only using the "sintering pulses" shown in Fig.1b, and (e)(f) SP-LMS only using the "pressing pulses" (the major laser parameters for (a)(b) are the same as those for Fig.2a, while the major laser parameters for (c)(d) are the same as those for Fig.2c. For (e)(f), the "pressing pulse" energy is ~0.179 mJ/pulse and the pulse repetition rate is 3.125 kHz.)

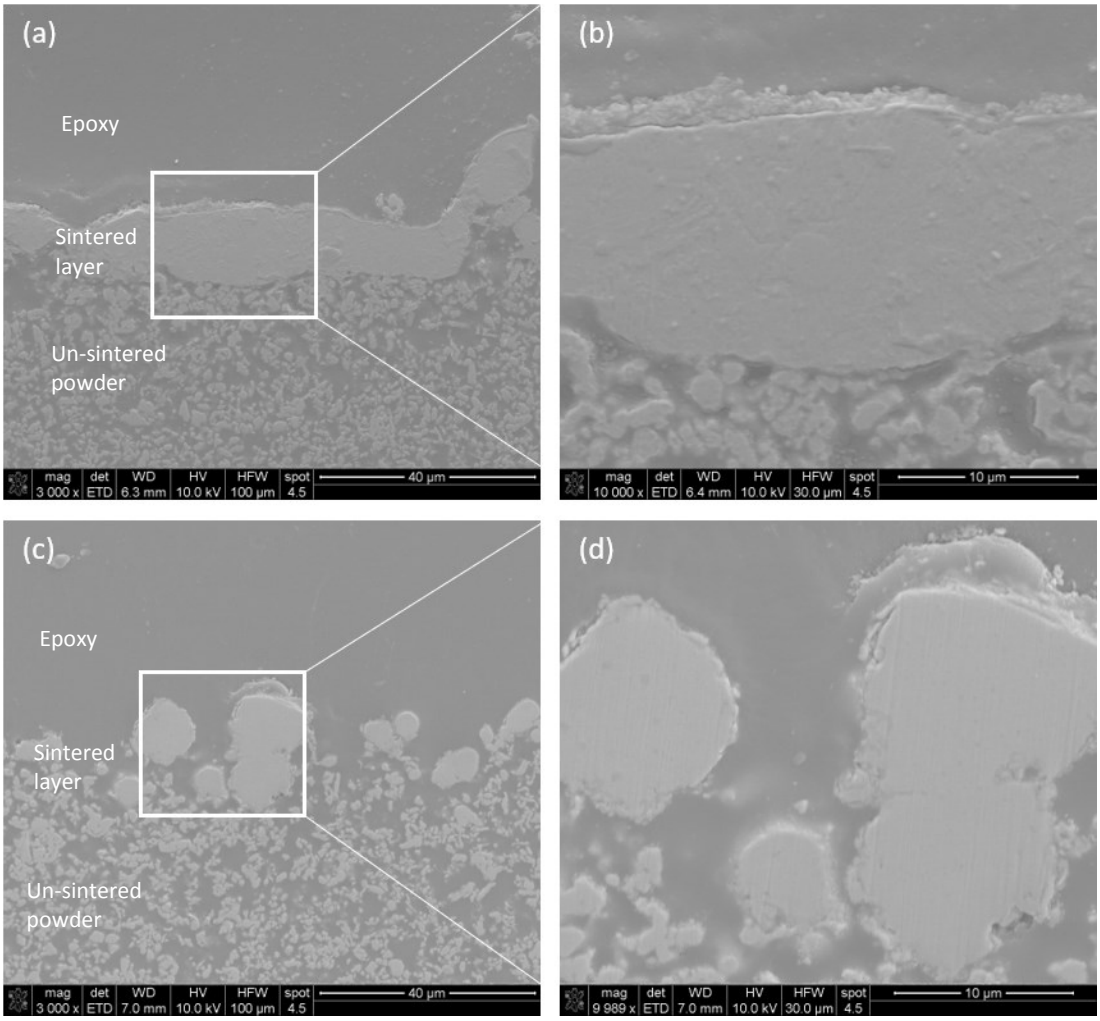

Figure 4. SEM images of the cross sections of samples sintered by: (a)(b) DP-LMS (with the same major laser parameters as those for Fig.2a) and (c)(d) SP-LMS only using the "sintering pulses" (with the same major laser parameters as those for Fig.2c).

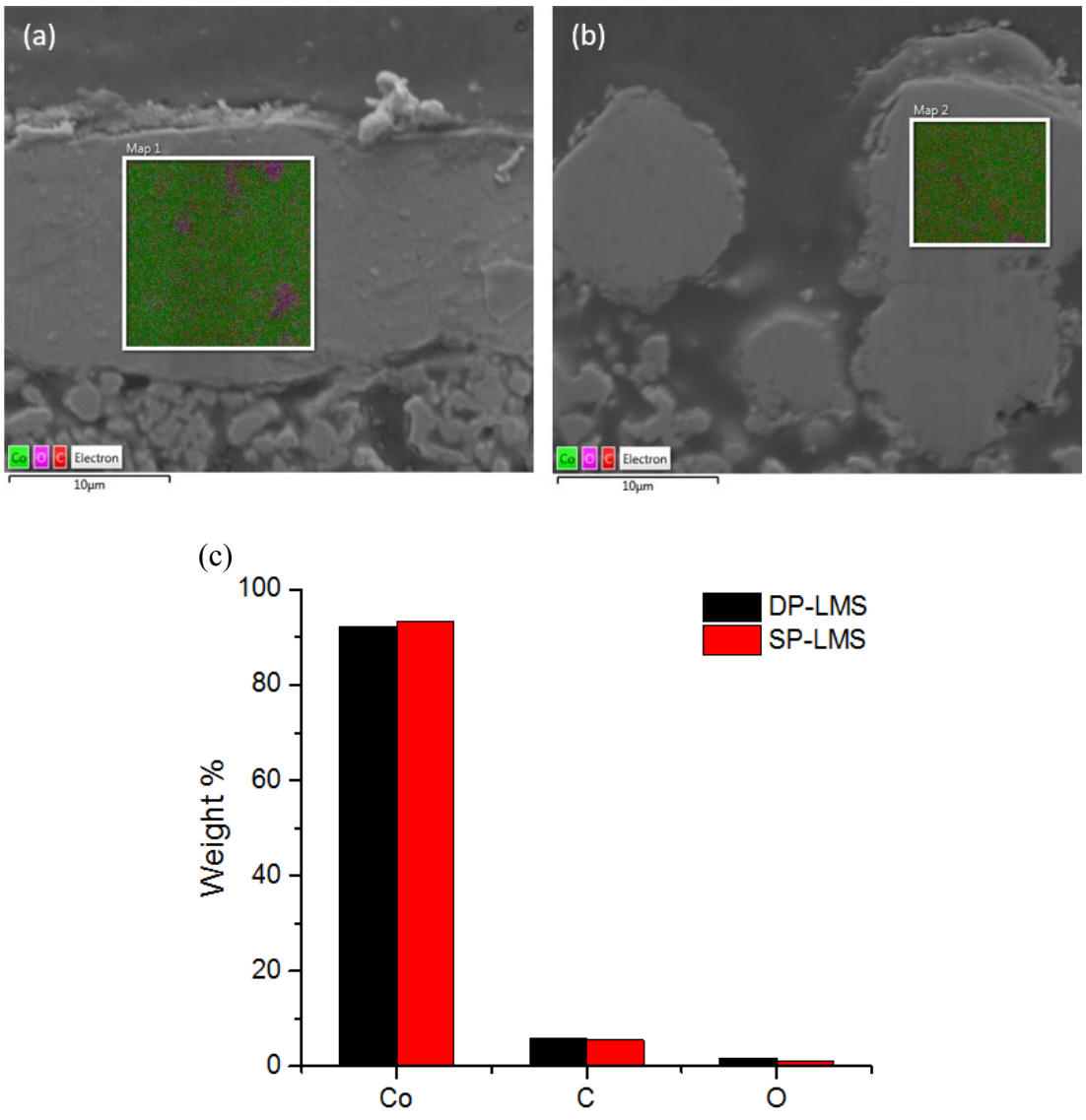

Figure 5. Elemental composition maps obtained from EDS measurements for cross-sectional regions of samples sintered by (a) DP-LMS (with the same major laser parameters as those for Fig.2a) and (b) SP-LMS with only the "sintering pulses" (with the same major laser parameters as those for Fig.2c); (c) the weight percentages of elements for the measured regions in (a) and (b).

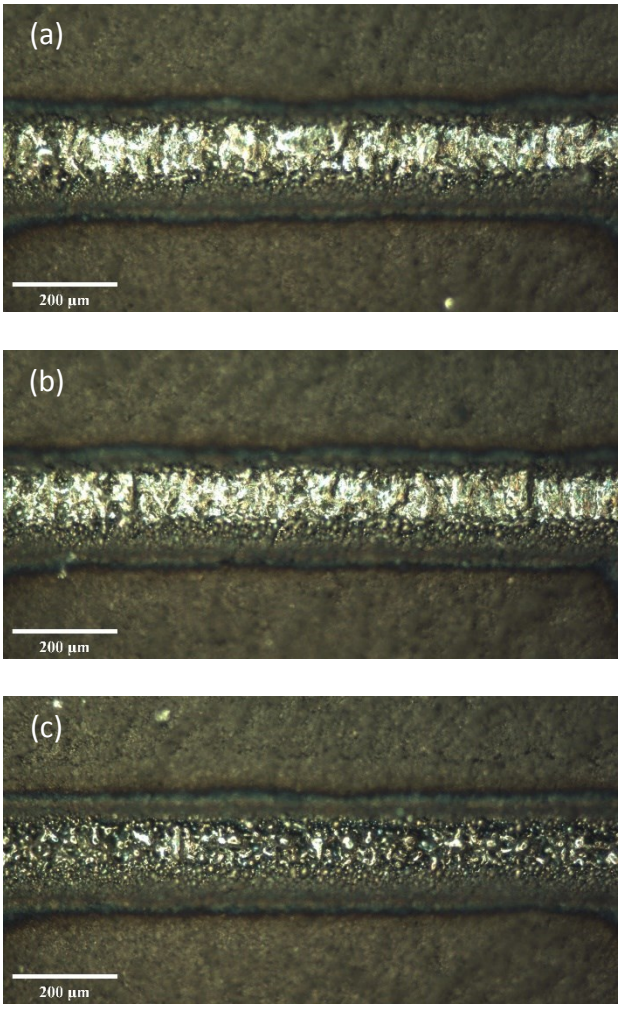

Figure 6. Optical microscope images of a portion of the material lines sintered by DP-LMS with different "pressing laser pulse" delay times: (a) τ_p = 25µs, (b) τ_p = 125µs and (c) τ_p = 625µs (average "sintering laser pulse" energy E_1 = ~0.067mJ, "pressing laser pulse" energy E_2 = ~0.179mJ, adjacent pulse group temporal distance τ_{gg} = 1040 µs).

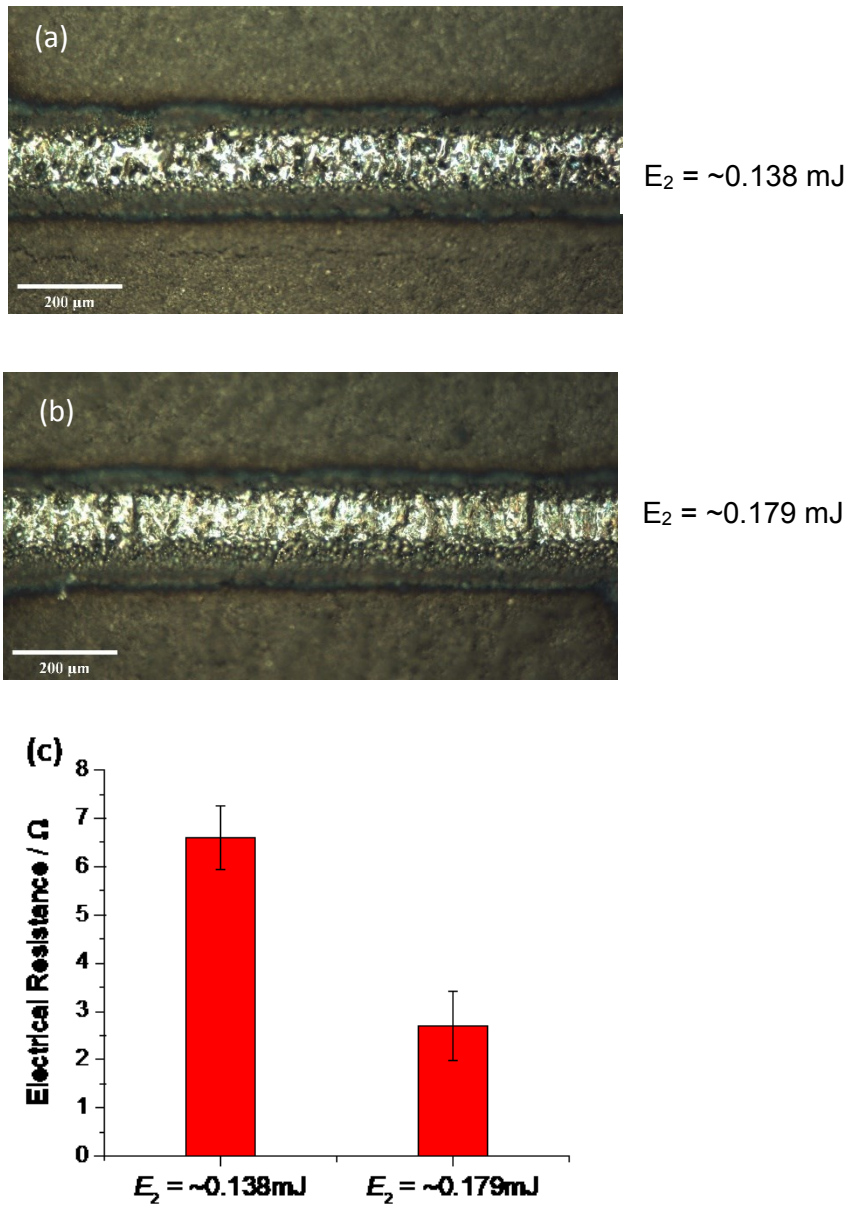

Figure 7. Optical microscopic images of a portion of material lines sintered by DP-LMS with different "pressing laser pulse" energies: (a) E_2 = ~0.138 mJ and (b) E_2 = ~0.179 mJ (average "sintering laser pulse" energy E_1 = ~0.067mJ, "pressing pulse" delay time τ_p = 125 µs, and adjacent pulse group temporal distance τ_{gg} = 1040 µs); (c) the average electrical resistances of material lines sintered by DP-LMS with the same major laser parameters as those for (a) and (b), respectively.

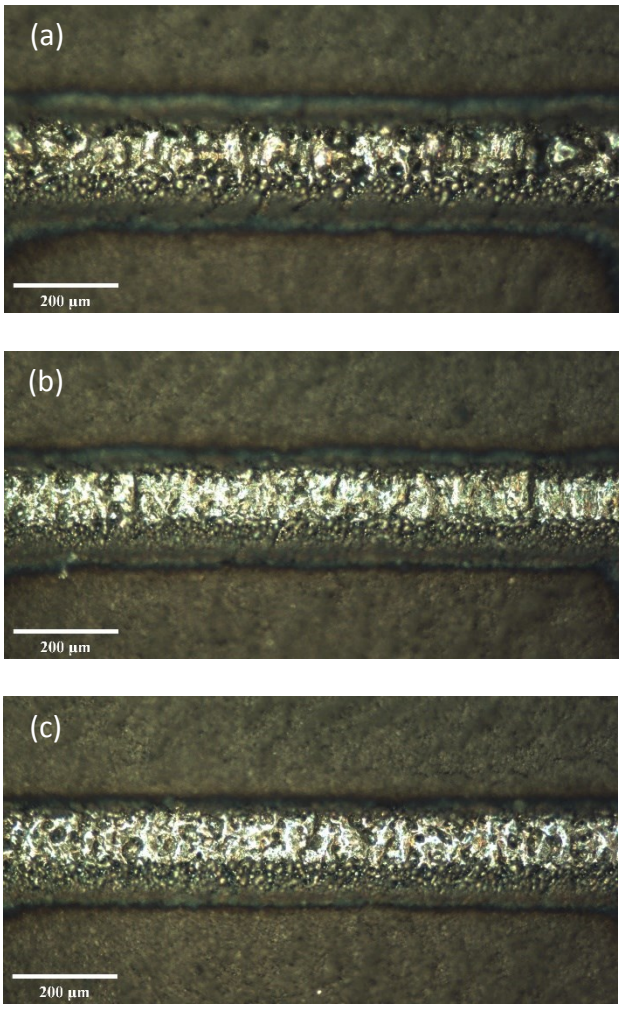

Figure 8. Optical microscopic images of a portion of material lines sintered by DP-LMS with different temporal distances between adjacent laser pulse groups (a) τ_{gg} = 640 µs; (b) τ_{gg} = 1040 µs; and (c) τ_{gg} = 1440 µs (average "sintering laser pulse" energy E_1 = ~0.067 mJ, "pressing laser pulse" energy E_2 = ~0.179 mJ, and "pressing pulse" delay time τ_p = 125 µs).

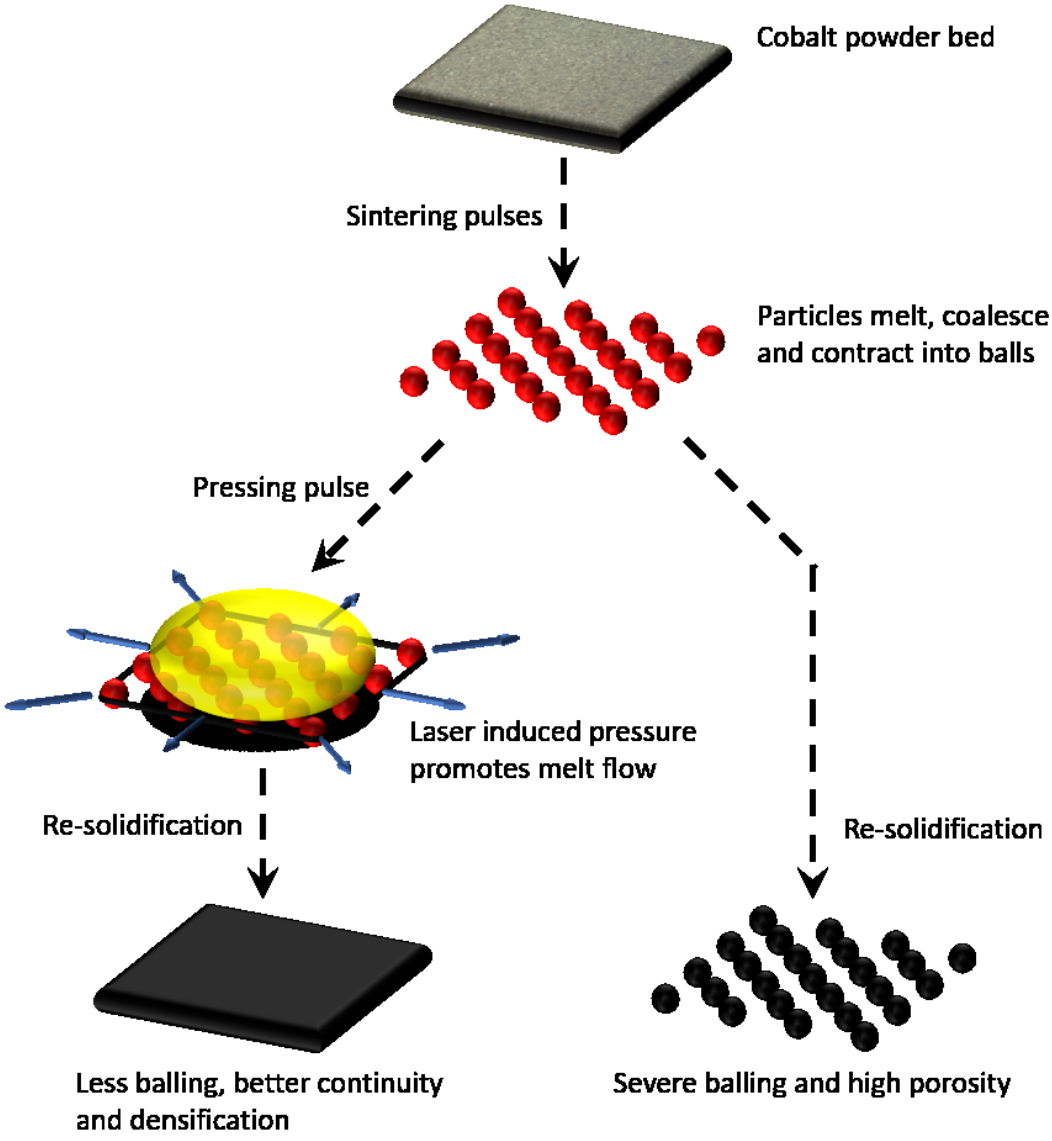

Figure 9. Schematic diagram of the potential fundamental mechanism for the different sintering results by DP-LMS and by SP-LMS with only the "sintering laser pulses" under the conditions studied.

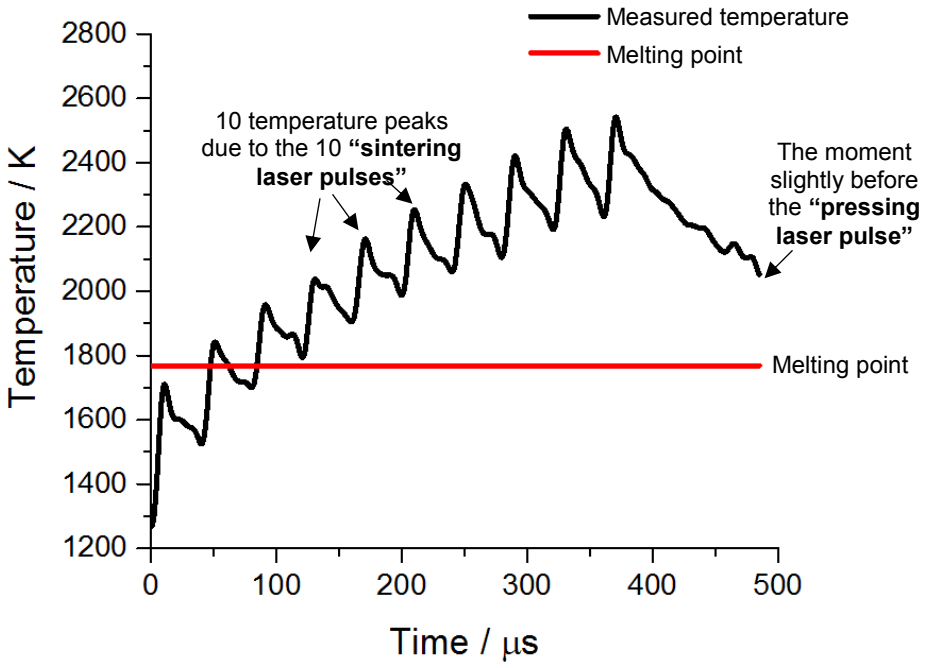

(a)

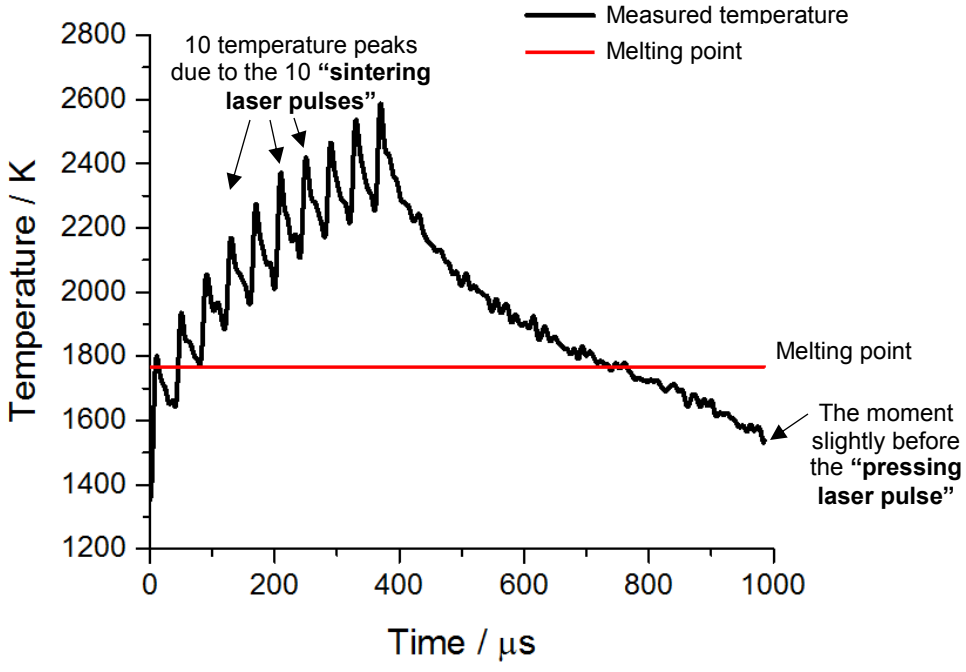

(b)

Figure 10. Powder bed surface temperature histories measured in situ during DP-LMS with a "pressing laser pulse" delay time of (a) τ_p = 125 μs and (b) τ_p = 625 μs (the other major laser parameters are the same as those for Fig.6).